On the onset of convective instabilities in cylindrical cavities heated from below. I. Pure thermal case

R. Touihri, H. Ben Hadid, and D. Henry
Laboratoire de Mécanique des Fluides et d'Acoustique—UMR CNRS 5509, Ecole Centrale de Lyon/ Université Claude Bernard-Lyon 1, ECL, BP 163, 69131 Ecully Cedex, France

(Received 12 August 1998; accepted 30 March 1999)

Three-dimensional steady flows are simulated in a circular cylindrical cavity of aspect ratio $A=H/D$, where H is the height and D the diameter of the cavity. The cavity is heated from below and its sidewalls are considered to be adiabatic. The effect of the geometry of the cavity on the onset of convection and on the structure and symmetries of the flow is analyzed. The nonlinear evolution of the convection beyond its onset is presented through bifurcation diagrams for two typical aspect ratios $A=0.5$ and $A=1$. Axisymmetric ($m=0$) and asymmetric ($m=1$ and $m=2$) azimuthal modes [$\exp(im\phi)$] are observed. For $A=0.5$, the axisymmetric solution loses its stability to a three-dimensional solution at a secondary bifurcation point. Better understanding of the mechanisms leading to this instability is obtained by analyzing the energy transfer between the basic state and the critical mode. To study the influence of the Prandtl number on the flow pattern and on the secondary bifurcation, three values of the Prandtl number are investigated: Pr=0.02 (liquid metal), Pr=1 (transparent liquids), and Pr=6.7 (water). © *1999 American Institute of Physics.* [S1070-6631(99)01907-8]

I. INTRODUCTION

Deep understanding of fluid motion is crucial in material processing technologies such as crystal growth. It is well known that such phenomena as the onset of convective instabilities and the transition to nonperiodic or periodic motions in the melt can destroy the homogeneity of crystals. Our work on the Rayleigh–Bénard instability in a cylinder is connected to these preoccupations, even if this particular instability has no direct relevance to any crystal-growth process: in the closest situation, the vertical Bridgman configuration, convection sets in first because of the radial temperature gradient, which is always present in such a process.

Rayleigh–Bénard[1,2] instability has been the subject of a large number of papers which have shown the importance that the control of the boundary conditions and the geometry of the container may have on the threshold values and the observed flow patterns. Compared to the buoyant flow between parallel planes of infinite extent, the circular cylindrical problem has received less attention, probably because of the complications introduced by the lateral boundaries. For this configuration, the analysis of the primary instabilities of the static diffusive solution has been well known since the works of Charlson and Sani,[3,4] Stork and Müller,[5] Rosenblat,[6] and Buell and Catton.[7] All these works have shown that the structure of the emerging flow, which is given by the first primary threshold, depends on the aspect ratio A ($A=H/D=$height/diameter). A transition between an asymmetric one-roll mode $m=1$ (solution for large values of A) and an axisymmetric mode $m=0$ occurs around $A=0.55$ for adiabatic sidewalls and $A=0.72$ for conductive sidewalls.

However, the study of the convection beyond its onset and secondary instabilities have been explored only for a few cases. The first numerical investigation of the stability of the axisymmetric solution, for small aspect ratio, is due to Charlson and Sani.[8] They expand the disturbances into the same set of basis functions as the ones used for the linear analysis. However, they failed in predicting the secondary instability, since the mode truncation was too severe. Müller *et al.*[9] investigated the flow patterns both numerically and experimentally for Pr=0.02 (liquid metal) and Pr=6.7 (water). The experiment, with water, showed that the axisymmetric solution loses its stability to a $m=1$ perturbation at $\mathrm{Ra}c_2 \simeq 10\mathrm{Ra}c_1 = 361\,600$. But numerically, for $A=0.5$, Pr=6.7, and Ra=44 800, they found an asymmetric two-roll stable solution, result confirmed by Neumann.[10] Hardin and Sani[11] approximated numerically the perturbed solution by retaining only the six most significant modes for $A=0.5$, and identified a secondary bifurcation at the critical Rayleigh number $\mathrm{Ra}c_2=45\,800$ for Pr=6.7, and $\mathrm{Ra}c_2=38\,880$ for Pr=0.02. For both cases, the unstable eigenvector corresponded to the mode $m=2$. Wagner *et al.*[12] simulated numerically the flow for $A=0.5$ and Pr=6.7, and, in contradiction with Neumann,[10] they found that the axisymmetric solution was stable at Ra=44 800. Recently, Wanschura *et al.*[13] made a complete analysis of this secondary instability. The study has been done in a range of aspect ratio for which the first primary threshold corresponds to the mode $m=0$. They confirmed that, in opposition to the primary instabilities for which the thresholds are independent of the Prandtl number, the secondary threshold increases with the Prandtl number, and depends also strongly on the aspect ratio. The unstable mode corresponding to this secondary transition is generally a mode $m=2$, but it can also be a mode $m=1$, 3 or 4. For

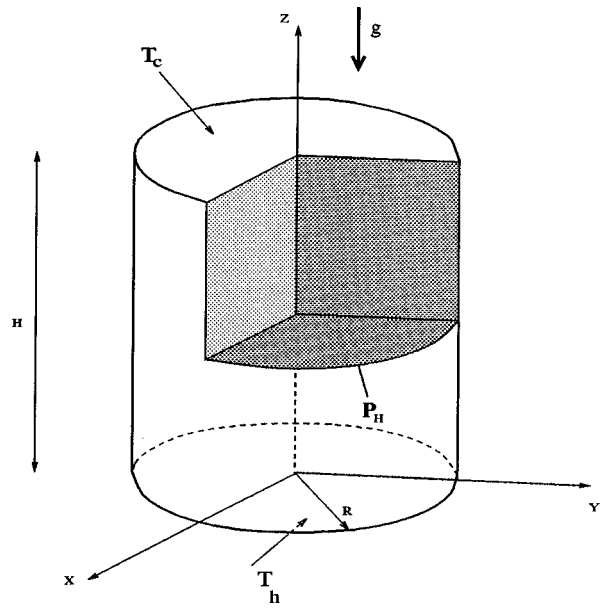

FIG. 1. Cavity configuration.

Pr=6.7, the axisymmetric solution is stable to the $m=2$ perturbation, and it becomes unstable to a mode $m=1$ at $\mathrm{Ra}c_2=162\,144$. Note that all these values of Ra are based on the diameter of the cavity and not on its height.

Analyses of symmetry in convective flows can be found in Refs. 14 and 15. The number of solutions appearing at a bifurcation can be directly related to the number of broken symmetries, because the image of a solution by a broken symmetry is also a solution. For the cylindrical geometry, the group of symmetries is called $\mathcal{O}(2)\times\mathcal{Z}(2)$, where $\mathcal{O}(2)$ contains all the rotations around the z axis and the reflections with respect to the vertical planes containing this axis, and $\mathcal{Z}(2)$ corresponds to the reflection with respect to the horizontal midplane.

Our purpose is the better understanding of the instabilities of the convective flow in a cylindrical cavity heated from below. We use a continuation method which is appropriate for the determination of the primary thresholds and the study of convection beyond its onset. The effect of the geometry of the cavity on the onset of the convection is presented by stability curves giving the evolution of the primary thresholds as a function of the aspect ratio. The evolution of the stable and unstable convective solutions beyond the primary thresholds is given through bifurcation diagrams for $A=0.5$ and $A=1$. For $A=0.5$, the energy transfer between the basic flow and the critical mode is analyzed, around the secondary bifurcation, in order to understand the mechanisms leading to this instability. Three values of the Prandtl number are investigated: 0.02, 1, and 6.7.

II. MATHEMATICAL MODEL

We consider an incompressible Newtonian fluid confined in a vertical cylindrical cavity of aspect ratio $A=H/D$, where H is the height and D the diameter (Fig. 1). The two ends of the cylinder are assumed isothermal. The lower end is held at temperature T_h, which is greater than the temperature T_c of the upper end, and the sidewalls are considered to be adiabatic. All the physical characteristics are taken as constant, except the density which varies linearly with temperature in the buoyancy term, $\rho=\rho_0(1-\beta(T-T_0))$ (Boussinesq approximation), where β is the thermal expansion coefficient and T_0 the mean temperature, $T_0=(T_h+T_c)/2$.

The governing equations for the temperature T, the pressure p, and the velocity $\boldsymbol{u}$ are the Navier–Stokes equations coupled with the energy equation. By scaling length by the diameter D of the cylinder, time by D^2/ν, velocity by $U_{\mathrm{ref}}=\nu\cdot\mathrm{Gr}/D$, and by introducing the dimensionless temperature field $\theta=A(T-T_0)/(T_h-T_c)$, the equations can be written in their dimensionless form as

$$\frac{\partial \boldsymbol{u}}{\partial t}=-\mathrm{Gr}(\boldsymbol{u}\cdot\boldsymbol{\nabla})\boldsymbol{u}-\boldsymbol{\nabla}p+\boldsymbol{\nabla}^2\boldsymbol{u}+\theta\hat{z}, \tag{1}$$

$$\nabla\cdot\boldsymbol{u}=0, \tag{2}$$

$$\frac{\partial\theta}{\partial t}=-\mathrm{Gr}\cdot\boldsymbol{u}\cdot\boldsymbol{\nabla}\theta+\frac{1}{\mathrm{Pr}}\cdot\boldsymbol{\nabla}^2\theta, \tag{3}$$

where $\mathrm{Gr}=(g\beta(T_h-T_c)D^4)/H\nu^2$, and $\mathrm{Pr}=\nu/\kappa$ are respectively the Grashof and the Prandtl numbers. We can also define the Rayleigh number as $\mathrm{Ra}=\mathrm{Gr}\cdot\mathrm{Pr}$. In these relations, κ is the thermal diffusivity and ν the kinematic viscosity. Note that, contrary to main previous studies, Gr and Ra have been based on D and not on H.

For the boundary conditions, the no-slip velocity boundary condition is prescribed at all the container walls, the temperature is fixed at the top and the bottom, and along the lateral wall ($r=R$), the normal heat flux is zero. Therefore, in their dimensionless form, the boundary conditions can be written as follows:

$$at\ \ r=1/2,\quad u=v=w=0,\quad \frac{\partial\theta}{\partial n}=0, \tag{4}$$

$$at\ \ z=0,\quad u=v=w=0,\quad \theta=A/2, \tag{5}$$

$$at\ \ z=A,\quad u=v=w=0,\quad \theta=-A/2. \tag{6}$$

Setting $\boldsymbol{u}=0$, we obtain the temperature profile of the static solution, $\theta(z)=(A/2-z)$, which corresponds to the diffusive regime.

III. NUMERICAL METHODS

To solve the governing equations, we use two different methods: direct numerical simulation, i.e., time stepping, and Newton's method. Time stepping has the ability to find the stable solutions, steady or oscillatory, with no restrictions on the initial conditions. Newton's method allows us to find either stable or unstable solutions, but only steady ones. To study the nonlinear evolution of the convection beyond its onset and determine the branches of steady solutions, we use a continuation method. This method is extended to the direct computation of the primary bifurcations to a steady state, as in Ref. 16.

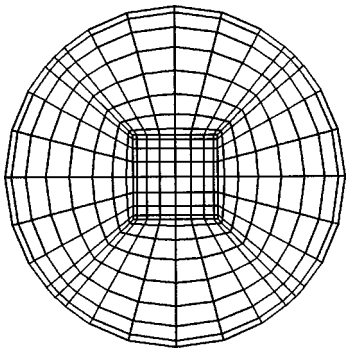

FIG. 2. Space discretization: the cavity is divided into five macro-elements (use of the isoparametric spectral element method).

A. Time stepping

Using a mixed implicit/explicit formulation to integrate the equations (1) and (3) over one time step, we get

$$\frac{\boldsymbol{u}^{n+1}-\boldsymbol{u}^{n}}{Dt} = -\mathrm{Gr}(\boldsymbol{u}^{n}\cdot\boldsymbol{\nabla})\boldsymbol{u}^{n} - \boldsymbol{\nabla} p^{n+1} + \boldsymbol{\nabla}^{2}\boldsymbol{u}^{n+1} + \theta^{n}\hat{z} \tag{7}$$

$$\frac{\theta^{n+1}-\theta^{n}}{Dt} = -\mathrm{Gr}(\boldsymbol{u}^{n}\cdot\boldsymbol{\nabla})\theta^{n} + \frac{\boldsymbol{\nabla}^{2}\theta^{n+1}}{Pr}. \tag{8}$$

Here, $\boldsymbol{u}^{n}$ and θ^{n} respectively are the discretized dimensionless values of the velocity and the temperature at time $t^{n}=nDt$, and Dt is the time step. The scheme presented is of first order, but for the direct numerical simulation we use the third-order version. The main idea of the splitting method we use to solve (7) and (8) (Ref. 17) is to decompose each time step into three substeps. We first treat the nonlinear terms explicitly. We then compute the pressure by solving a spectral elliptic problem with Neumann boundary conditions depending on the nonlinear term. The resolution of the pressure field insures the incompressibility of the final field $\boldsymbol{u}^{n+1}$ which is calculated at the third substep by treating implicitly the linear terms and solving a Helmholtz problem with appropriate Dirichlet boundary conditions.

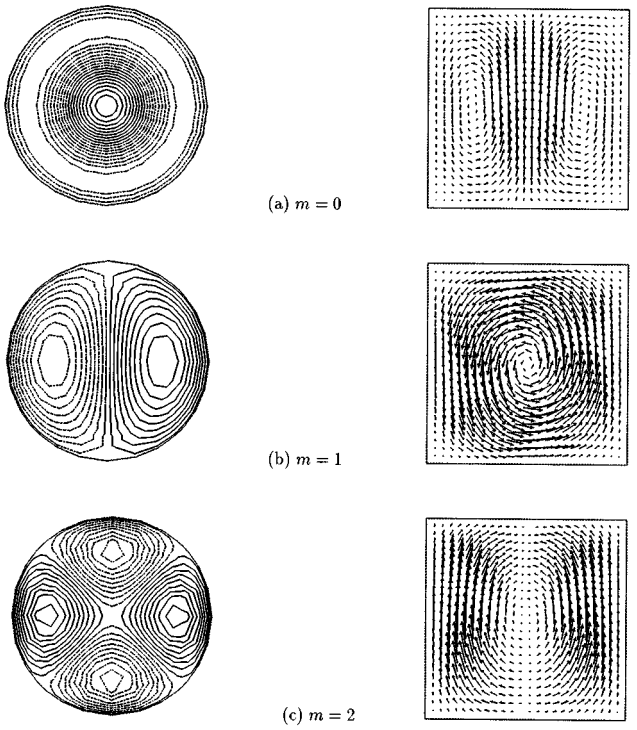

FIG. 3. The three principal modes, (a) $m=0$, (b) $m=1$, and (c) $m=2$. Left-hand side: contours of the vertical velocity w in the horizontal midplane P_H. Right-hand side: velocity field in a vertical midplane ($A=1$).

TABLE I. Tests of numerical accuracy for the pure thermal case (Ra $=4.10^{4}$, Pr$=1$, and $A=0.5$).

n_x+1	n_y+1	n_z+1	$w_{\max}$	Ec	Nu
7	7	9	0.3304×10^{-3}	$0.172\,98\times10^{-8}$	1.068 50
9	9	9	0.3299×10^{-3}	$0.172\,40\times10^{-8}$	1.066 70
9	9	11	0.3293×10^{-3}	$0.171\,64\times10^{-8}$	1.068 31

B. Newton solver

Let $\boldsymbol{U}$ denote $(\boldsymbol{u},\theta)$, $N(\boldsymbol{U})=(-(\boldsymbol{u}\cdot\boldsymbol{\nabla})\boldsymbol{u}-\boldsymbol{\nabla}p,-\boldsymbol{u}\boldsymbol{\nabla}\theta)$ and $L(\boldsymbol{U})=(\boldsymbol{\nabla}^{2}u,\boldsymbol{\nabla}^{2}\theta)$, so that the equations (7) and (8) can be written as

$$\boldsymbol{U}^{n+1}-\boldsymbol{U}^{n} = Dt(\mathrm{Gr}\cdot N(\boldsymbol{U}^{n})+L(\boldsymbol{U}^{n+1})), \tag{9}$$

or

$$\boldsymbol{U}^{n+1}-\boldsymbol{U}^{n} = (I-Dt\cdot L)^{-1}(\mathrm{Gr}\cdot N+L)\boldsymbol{U}^{n}. \tag{10}$$

If we consider

$$f(\boldsymbol{U},\mathrm{Gr}) = (\mathrm{Gr}\cdot N+L)\boldsymbol{U}, \tag{11}$$

then the steady solutions ($\boldsymbol{U}$, Gr) can be calculated by solving $f(\boldsymbol{U},\mathrm{Gr})=0$. This equation is solved by Newton's method, with $\mathbf{P}=(\mathbf{I}-\mathbf{DtL})^{-1}$ used as a preconditioner. At each Newton step k, we then get the following linear system:

$$\mathbf{P}D_{\boldsymbol{U}}f(\boldsymbol{U}^{k},\mathrm{Gr}^{k})\cdot\delta\boldsymbol{U}^{k}+\mathbf{P}D_{\mathrm{Gr}}f(\boldsymbol{U}^{k},\mathrm{Gr}^{k})\,\delta\mathrm{Gr}_{k} = -\mathbf{P}f(\boldsymbol{U}^{k},Gr^{k}), \tag{12}$$

which is solved by the biconjugate gradient squared method.[18] The number of Newton iterations required to obtain the final solution depends essentially on the accuracy we require for the biconjugate gradient squared method at each Newton iteration. Referring to (10), we see that the right- and left-hand sides of (12) can be calculated by carrying out time steps (see details in Refs. 19 and 16).

C. Continuation method

In order to study the nonlinear evolution of the convection, we have to determine the evolution of the unknowns

TABLE II. Comparison of the critical Rayleigh numbers for the onset of convection, for $A=0.5$ and $A=1$, with the results of previous linear stability analyses.

A	Charlson *et al.* (Ref. 4)	Gershuni *et al.* (Ref. 25)	Buell *et al.* (Ref. 7)	Neumann (Ref. 10)	Present work
0.5	36 160	36 000	36 160	35 520	35 854
1	4500	3900	3800	3610	3696

TABLE III. Critical Rayleigh numbers corresponding to the first primary thresholds for $A=0.5$ and $A=1$.

Mode	$m=0$	$m=2$	$m=1$
$A=0.5$	35 854	38 928	41 783
$A=1$	10 752	8939	3696

$\mathbf{U}(\boldsymbol{u},\theta)$ when the Rayleigh number (or the Grashof number) is increased beyond the primary thresholds. The continuation method is used to construct the branches of steady solutions step by step. These solutions are characterized by the relation $f(\boldsymbol{U},\mathrm{Gr})=0$. Each step of continuation is divided into two substeps: prediction and correction. From a given solution $(\boldsymbol{U}_s,\mathrm{Gr}_s)$, we first predict $(\boldsymbol{U}_p,\mathrm{Gr}_p)$ closer to a new solution. This prediction depends on the number of the solutions already calculated: we extrapolate linearly if we have two solutions and quadratically if we have more. Then, we apply Newton's method to correct the prediction and calculate a new solution $(\boldsymbol{U}_{s+1},\mathrm{Gr}_{s+1})$.[20] This correction is usually made by fixing the Grashof number $(\mathrm{Gr}_{s+1}=\mathrm{Gr}_p)$, except close to pitchfork bifurcations or saddle-node points.[16,21]

To check the stability of the branches of solutions, we use Arnoldi's method. We calculate a Hessenberg matrix whose eigenvalues and eigenvectors are the leading modes of the full Jacobian of the governing equations. This Hessenberg matrix, of much lower dimension than the Jacobian, is easy to diagonalize.[22]

The continuation method combined with Newton's solver is also used to calculate the stability diagrams. This allows us to follow the evolution of the primary thresholds, even if the corresponding eigenvectors are not the most unstable modes.

D. Space discretization and accuracy

For the spatial discretization, we use an isoparametric multidomain pseudo-spectral method.[23,24] The computational domain is divided into five macro-elements (Fig. 2), and the solution (u,v,w,θ), in the Cartesian coordinates (x,y,z), is represented in each element as a high-order Lagrangian interpolant through a Legendre–Gauss–Lobatto points distribution. To study the effect of the grid on the numerical accuracy, we give in Table I the values of the maximum of the vertical velocity $w_{\max}$, the kinetic energy E_c, and the Nusselt number Nu for different meshes. When the grid is refined from $7\times7\times9$ to $9\times9\times9$ mesh points per element (respectively for the *x*, *y*, and *z* directions), the maximum of variation concerns the kinetic energy *Ec* and is equal to 0.82%. A further increase of the number of grid points per element from $9\times9\times9$ to $9\times9\times11$ shows that the maximum

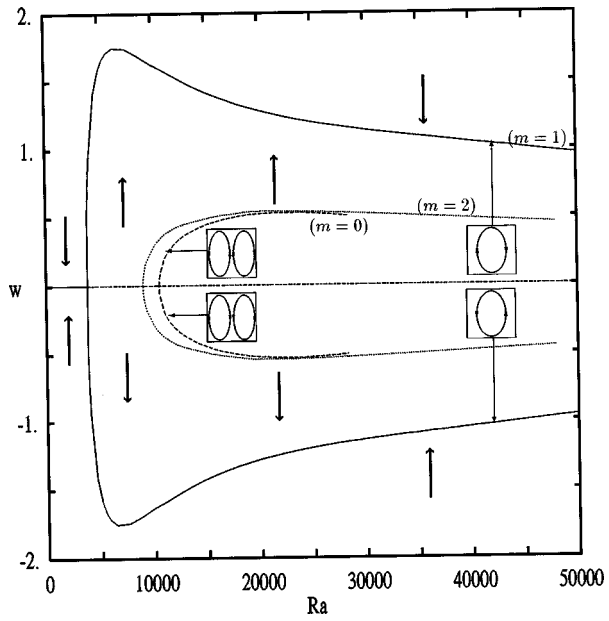

FIG. 5. Bifurcation diagram giving the evolution of the vertical velocity *w* at a fixed point as a function of the Rayleigh number, Ra ($A=1$ and $\mathrm{Pr}=1$).

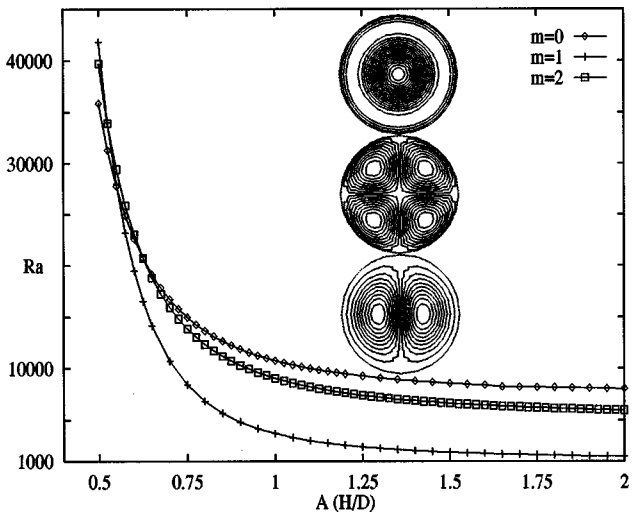

FIG. 4. Influence of the aspect ratio on the onset of convection. Evolution of the primary thresholds Ra_c, corresponding to the modes $m=0$, $m=1$, and $m=2$, as a function of *A*.

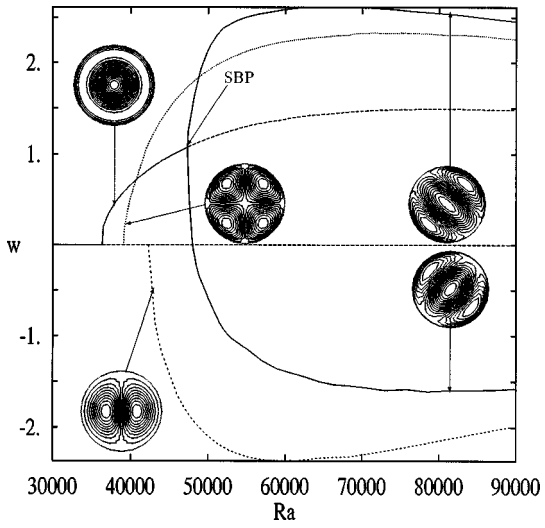

FIG. 6. Bifurcation diagram giving the evolution of the vertical velocity *w* at a fixed point as a function of the Rayleigh number, Ra. Plots of contours of *w* in the horizontal midplane. SBP: secondary bifurcation point ($A=0.5$ and $\mathrm{Pr}=1$).

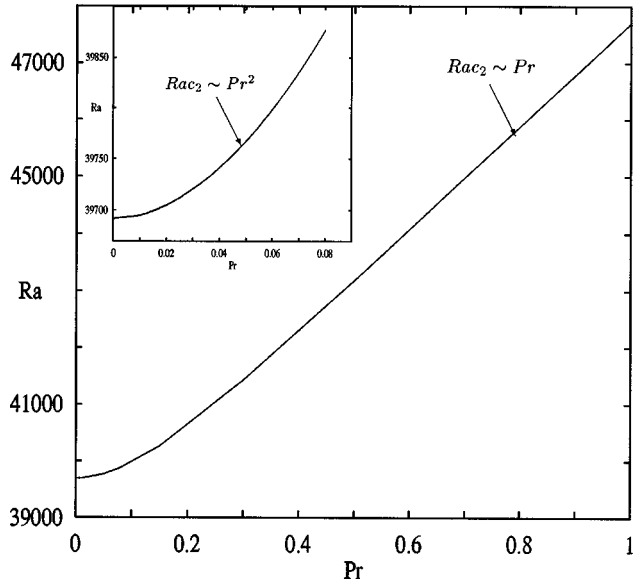

FIG. 7. Influence of the Prandtl number on the secondary bifurcation (from $m=0$ to $m=02$) for $A=0.5$. Evolution of the secondary threshold $\mathrm{Ra}c_2$ as a function of Pr.

of variation is also for E_c and equal to 0.44%. Therefore, the grid with $7\times7\times9$ points per element is considered sufficiently fine to study the pure thermal case.

IV. RESULTS

A. Onset of convection: linear analysis

1. Modes and symmetries

Convection arises when the temperature difference between the lower and upper surfaces $\Delta T=T_h-T_c$ exceeds a critical value given by the Rayleigh number, Ra. In the case of a circular cylindrical geometry, because of the specific lateral confinement, convection sets in as single Fourier modes in the azimuthal direction [variation in $\exp(im\phi)$ of these modes]. We present in Fig. 3 the most important modes, which correspond to $m=0$ (axisymmetric solution), $m=1$, and $m=2$ (asymmetric solutions). At the primary bifurcations, the corresponding modes can be characterized by their broken symmetries with regard to the symmetries of the problem. In fact, the number of solutions obtained at a bifurcation can be deduced from the number of broken symmetries, because every image of a solution by a broken symmetry is also solution. In the pure thermal case and for circular cylindrical geometry, the symmetries of the problem are: the rotations around the z axis, the reflections with respect to the vertical planes containing this axis, and the reflection with respect to the horizontal midplane P_H. This group of symmetries is commonly called "$\mathcal{O}(2)\times\mathcal{Z}(2)$"[14] and corresponds to the symmetry properties of the trivial solution.

For the axisymmetric mode, the flow is purely meridional and independent of the azimuthal direction. The only broken symmetry is the reflection with respect to the horizontal mid-plane P_H, so only two solutions can be obtained: the first is given in Fig. 3 and the second is its reflection with respect to the plane P_H. The second mode ($m=1$) is asymmetric with one roll. As shown by the contours of vertical velocity in the plane P_H, the fluid rises at one side and falls at the other side of the cylindrical container. The symmetries preserved are the reflection with respect to the single vertical plane in which there is no azimuthal motion, and the reflection with respect to the horizontal midline perpendicular to this plane. Thus the azimuthal rotation which is broken generates an infinite number of solutions. The third mode, which corresponds to the second Fourier mode ($m=2$), is asymmetric and characterized by its two orthogonal symmetry planes. All the other symmetries are broken, so, here also, an infinite number of equivalent solutions can be generated by symmetry operations. Contours of the vertical velocity in the plane P_H show that, for this mode, the fluid ascends in two opposite quadrants of the cylinder and descends in the two others.

TABLE IV. Comparison of the values of the secondary thresholds $\mathrm{Ra}c_2$ with the values given in the literature, for Pr=0.02 and Pr=1 ($A=0.5$).

Pr	Neumann (Ref. 10)	Hardin *et al.* (Ref. 11)	Wanschura *et al.* (Ref. 13)	Present work
0.02	40 400	38 880	39 408	39 705
1	65 600	⋯	48 272	47 508

2. Stability of the static solution

Linear stability analysis is performed about the static (or conductive) solution in order to evaluate the critical values of the Rayleigh number Ra_c at which the stability of this solution changes. At these points, referred to as primary bifurcation points, the static solution undergoes pitchfork bifurcations leading to branches of steady solutions. In agreement with the linear stability studies given in the literature (see Table II), convection sets in with the axisymmetric mode ($m=0$) for $A=0.5$ and with the asymmetric single-roll mode ($m=1$) for $A=1$. The next primary bifurcations correspond to the modes $m=2$ and $m=1$ for $A=0.5$, and to the modes $m=2$ and $m=0$ for $A=1$. In Table III, we present the values of the critical Rayleigh number for the three first primary thresholds corresponding to the modes $m=0$, 1, and 2.

3. Effect of the aspect ratio on the onset of convection

The stability diagram presented in Fig. 4 gives the evolution of the critical Rayleigh numbers Ra_c, corresponding to the primary bifurcations to the modes $m=0$, 1, and 2, as a function of the aspect ratio. For the first primary threshold which determines the structure of the emerging flow, the mode changes as A is increased. These changes happen at the intersections between the curves corresponding to a given mode. For $A<0.55$, convection sets in with the mode $m=0$ followed by the modes $m=2$ and $m=1$, whereas for $0.55<A<0.63$, the first mode is $m=1$ and the next are $m=0$ and $m=2$. Finally, for $A>0.63$, the order of appearance is $m=1$, $m=2$, and $m=0$. Beyond this value of A, the only effect of increasing A is a continuous decrease in Ra_c. An asymptotic critical value $\mathrm{Ra}_c\simeq1060$ (Ref. 7) exists for $A\rightarrow\infty$.

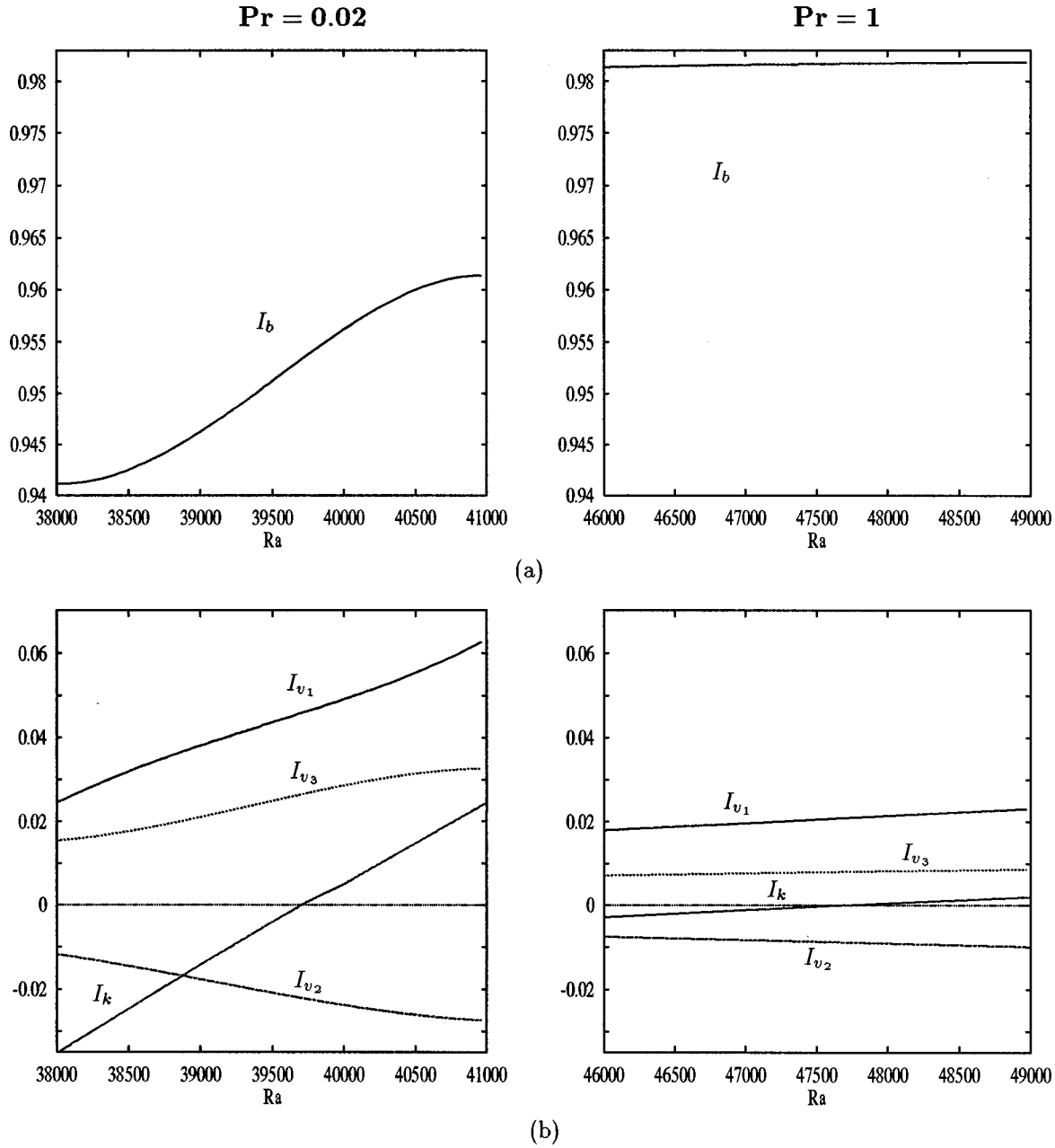

FIG. 8. Main kinetic energy contributions for Pr=0.02 and Pr=1, around the secondary bifurcation point. Evolution of the buoyancy term I_b (a), the rate of change of kinetic energy I_k, and the main kinetic energy production terms I_{v_1}, I_{v_2}, and I_{v_3} (b) as a function of Ra ($A=0.5$).

B. Evolution of the convection: Nonlinear analysis

The aim of this section is to study the nonlinear evolution of the steady convective regimes initiated at the primary thresholds. Convective flow patterns are calculated for two typical aspect ratios, $A=0.5$ and $A=1$. The results are given through bifurcation diagrams. In these diagrams, the evolution of the vertical velocity w at a fixed point is presented as a function of the Rayleigh number. The dependence of the convective behavior on the Prandtl number, Pr, is also investigated.

1. Bifurcation diagrams

For $A=1$ and Pr=1, as predicted by the linear analysis, convection sets in with a $m=1$ mode at the critical value Ra=3696. The second branch, which is unstable, corresponds to the mode $m=2$ and appears at Ra=8939. Finally, the $m=0$ branch, which is also unstable, appears at Ra =10 752. The symmetry of the bifurcation diagram shown in Fig. 5 with respect to the Ra axis confirms that all the primary bifurcations are pitchfork bifurcations. This is due to the fact that every primary bifurcation breaks the symmetry with respect to the horizontal midplane P_H. For the range of Rayleigh numbers investigated, no steady bifurcation of the flow structure has been detected.

The bifurcation diagram given in Fig. 6 has been obtained for $A=0.5$ and Pr=1. In this diagram we also give the contours of the vertical velocity in the plane P_H for the different branches of solutions. Above a critical value Ra

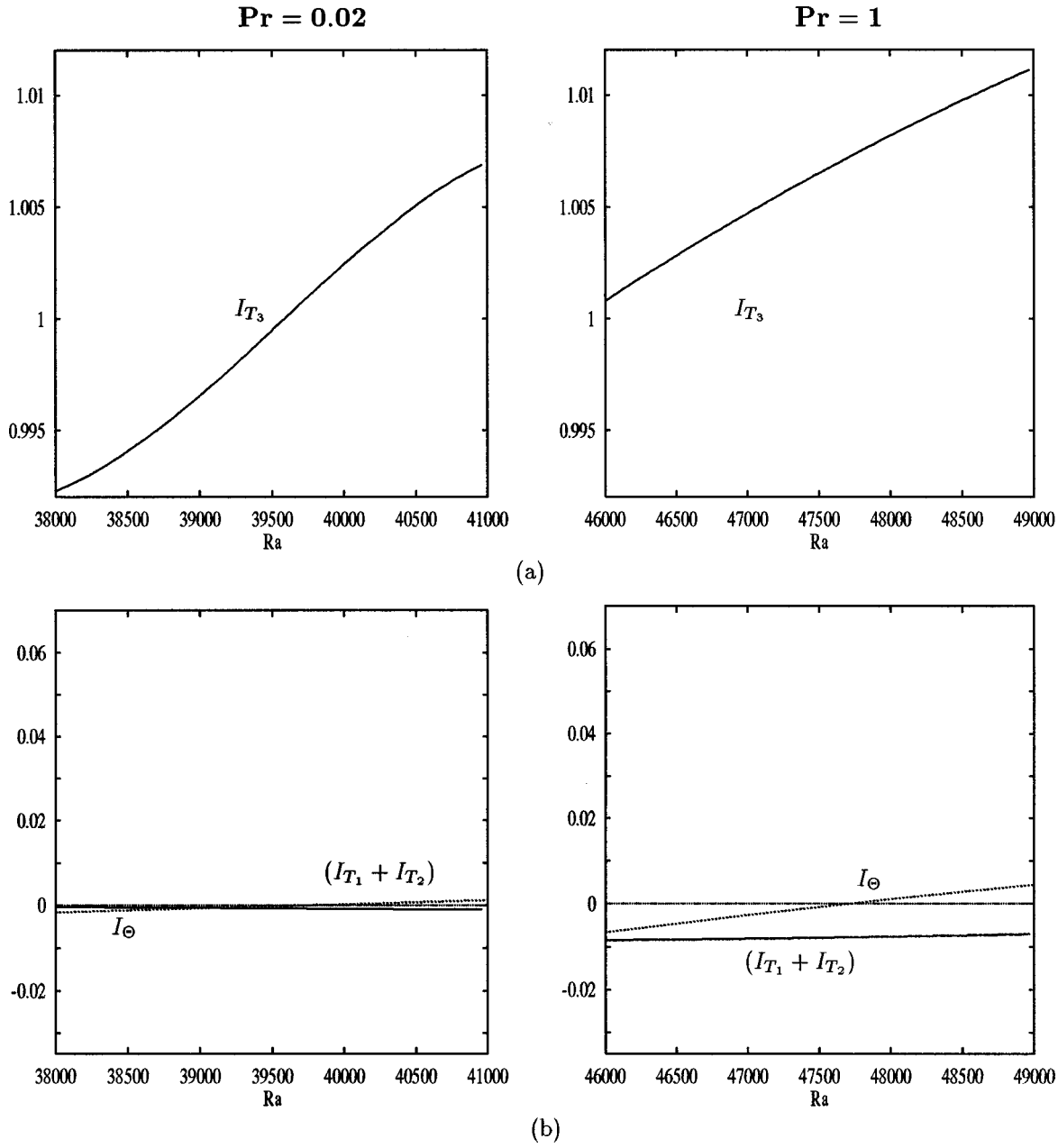

FIG. 9. Main thermal energy contributions for Pr=0.02 and Pr=1, around the secondary bifurcation point. Evolution of the thermal energy production terms I_{T_3} (a), $I_{T_1}+I_{T_2}$ and the rate of change of thermal energy I_Θ (b) as a function of Ra ($A=0.5$).

$=35\,854$, convection sets in with the axisymmetric mode ($m=0$). The second branch originates at Ra$=38\,928$ and corresponds to the mode $m=2$. Finally, the $m=1$ branch appears at Ra$=41\,783$.

2. Analysis of stability of the axisymmetric mode

An interesting feature of Fig. 6 is the destabilization of the axisymmetric solution at a secondary pitchfork bifurcation point at Ra$c_2=47\,508$. Above this critical value, the axisymmetric solution bifurcates to a new asymmetric mode which we call $m=02$. This mode can be described as a superposition of the basic mode $m=0$ and the mode of the unstable eigenvector $m=2$. The contour plot of the vertical velocity of the $m=02$ solution shows that it consists of two counter-rotating and parallel rolls. It should be noted that this bifurcation consists of a direct (not oscillatory) transition from a steady axisymmetric to a steady asymmetric convection. Only two symmetries are preserved: the reflections with respect to the two vertical central plane, parallel or perpendicular to the roll axes. Therefore, an infinite number of new stable branches of solutions (defined to within a rotation) are initiated at the secondary bifurcation point.

3. Effect of the Prandtl number on the secondary bifurcation

As it is well known, the primary thresholds do not depend on the Prandtl number. To study the influence of this number on the secondary bifurcation, we present in Fig. 7 the evolution of the secondary threshold, given by the corresponding critical Rayleigh number Rac_2, as a function of Pr.

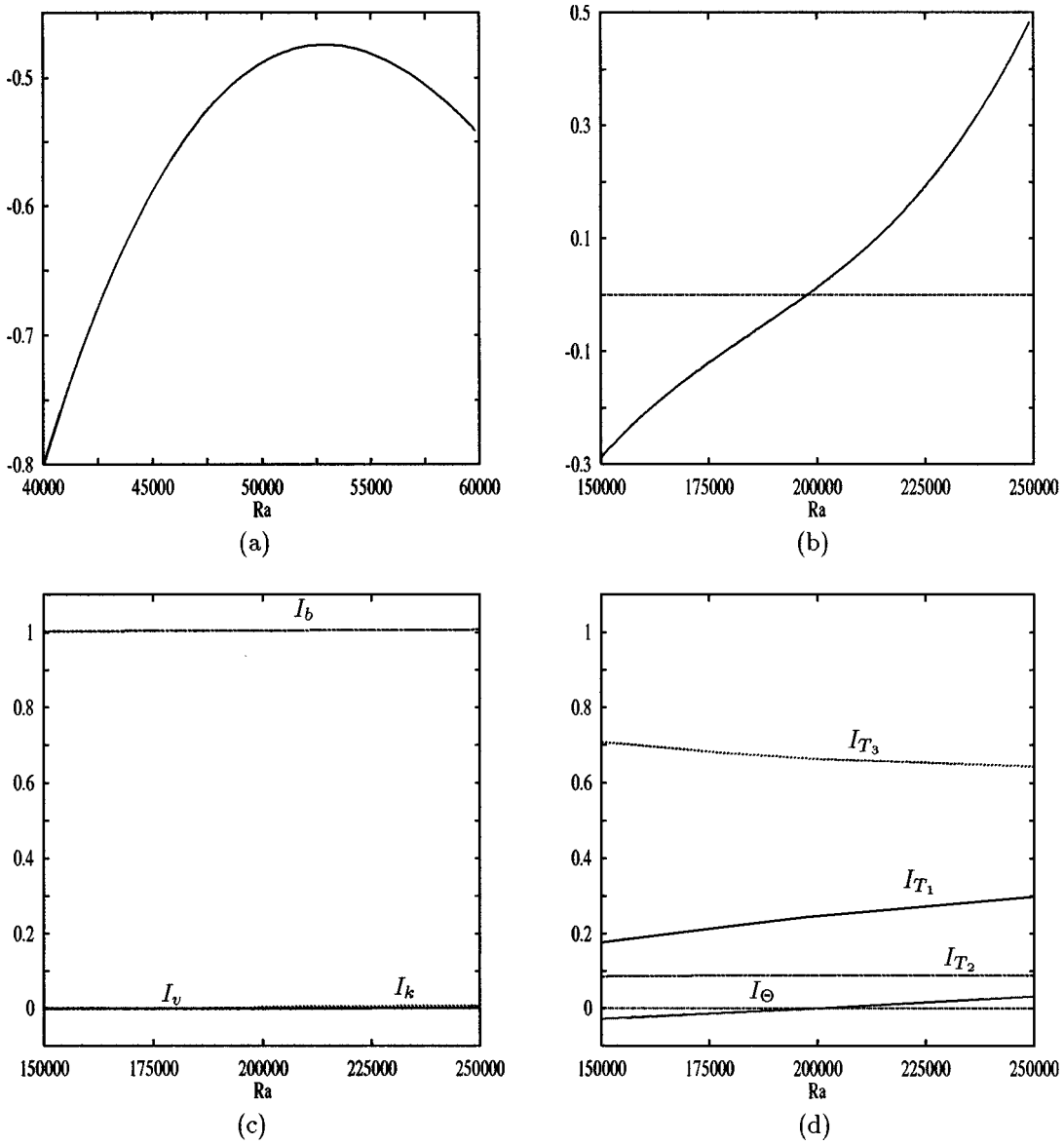

FIG. 10. Analysis of the secondary bifurcation for Pr=6.7 ($A=0.5$). Evolution of the critical eigenvalues corresponding to the mode $m=2$ (a) and the mode $m=1$ (b) as a function of Ra. Main kinetic energy contributions, I_b, I_k, and I_v (c), and thermal energy contributions, I_{T_1}, I_{T_2}, I_{T_3}, and I_Θ (d) as a function of Ra, around the secondary bifurcation point ($m=1$ perturbation).

This figure shows that $\mathrm{Ra}c_2$ increases with Pr, indicating that the axisymmetry of the flow disappears earlier for the low-Prandtl-number fluids. In the domain of study, this increase is mainly linear, except for the small values of Pr where it is quadratic. In Table IV, we compare our values of $\mathrm{Ra}c_2$ with the values given in the literature, for Pr=0.02 and Pr=1.

4. Energetic analysis of the secondary bifurcation

To understand the physical mechanisms responsible for the secondary instability, we analyze the energy transfer around the secondary bifurcation point. We decompose the field $(\boldsymbol{u},T)$ into a sum of two terms, $(\boldsymbol{u}_0,T_0)$ which is the basic axisymmetric field, and $(\boldsymbol{u}',T')$ the disturbance which, close to the transition, can be approximated by the unstable eigenvector. We first write the governing equations for $(\boldsymbol{u},T)$, then subtract those for the basic field. After multiplying the result by the disturbance, and integrating over the volume Ω of the cavity, we obtain

$$\frac{dk}{dt}=\frac{1}{2}\int_\Omega \frac{d}{dt}\,(u_i'u_i')\,d\Omega$$

$$=-\mathrm{Gr}\int_\Omega u_i'u_j'\,\frac{\partial u_0}{\partial x_j}\,d\Omega-\int_\Omega\left(\frac{\partial u_i'}{\partial x_j}\right)^2 d\Omega+\int_\Omega w'T'\,d\Omega, \tag{13}$$

$$\frac{d\Theta}{dt}=\frac{1}{2}\int_\Omega \frac{d}{dt}\,(T'^2)\,d\Omega$$

$$=-\mathrm{Gr}\int_\Omega T'v_i'\,\frac{\partial T_0}{\partial x_i}\,d\Omega-\frac{1}{\mathrm{Pr}}\int_\Omega\left(\frac{\partial T'}{\partial x_i}\right)^2 d\Omega, \tag{14}$$

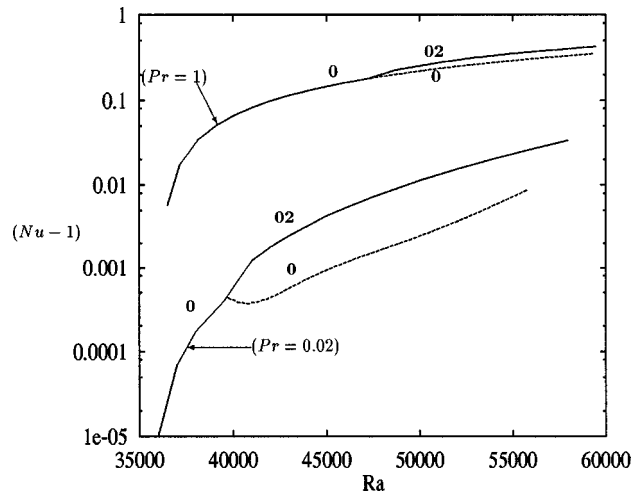

FIG. 11. Evolution of the Nusselt number, Nu, as a function of Ra, around the secondary bifurcation, for Pr=0.02 and Pr=1 ($A=0.5$).

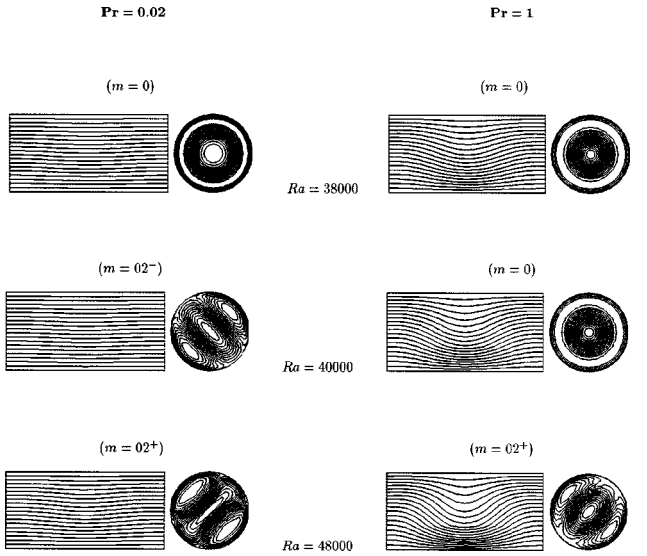

FIG. 12. Evolution of the convective structure of the steady stable solution for Pr=1 and Pr=0.02. Isotherms in the vertical symmetry plane and contours of the vertical velocity in the midplane P_H, before and after the secondary bifurcation from the mode $m=0$ to the mode $m=02$ ($A=0.5$).

where k and Θ denote respectively the kinetic and thermal energy due to the disturbance. These equations can be written respectively as

$$I_k = I_v + I_d + I_b, \tag{15}$$

$$I_\Theta = I_T + I_{dT}. \tag{16}$$

Here, I_k and I_Θ represent respectively the change of kinetic and thermal energies with respect to time. In the first equation, I_v is the sum of nine terms characterizing the interaction between the basic flow and the disturbance flow, I_d is the viscous dissipation of kinetic energy, and I_b measures the amplification of the temperature disturbance (T') by axial disturbance flow (w'). For the second equation, I_T is the sum of three terms giving the amplification of the temperature disturbance (T') by the transport in each direction of the heat flux of the basic solution ($\partial T_0/\partial x_i$), and I_{dT} gives the dissipation of heat. In our analysis, each term of the right-hand sides of the equations (15) and (16) is stabilizing if its sign is negative and destabilizing otherwise.

For the results presented in the following, all the terms are normalized by $|I_d|$ for the kinetic energy contributions and by $|I_{dT}|$ for the thermal energy contributions. Figure 8 giving the evolution of I_v, I_b, and I_k around the transition, for Pr=0.02 and 1, shows that the production of kinetic energy (I_v terms) is larger for Pr=0.02, even though I_b, which is greater for Pr=1, is the most destabilizing term for both cases.

The values of the three terms in I_v which are significant for the production of kinetic energy are plotted in Fig. 8(b) and are

$$I_{v_1} = I_{v_{13}} + I_{v_{23}} = -\mathrm{Gr}\int_\Omega \left(u'w' \frac{\partial u_0}{\partial z} + v'w' \frac{\partial v_0}{\partial z} \right) d\Omega, \tag{17}$$

$$I_{v_2} = I_{v_{31}} + I_{v_{32}} = -\mathrm{Gr}\int_\Omega \left(w'u' \frac{\partial w_0}{\partial x} + w'v' \frac{\partial w_0}{\partial y} \right) d\Omega, \tag{18}$$

$$I_{v_3} = -\mathrm{Gr}\int_\Omega \left(w'w' \frac{\partial w_0}{\partial z} \right) d\Omega. \tag{19}$$

Let (u_r, u_ϕ, w) denote the velocity components in the cylindrical coordinates. Using the axisymmetry of the basic solution, we can express I_{v_1} and I_{v_2} as

$$I_{v_1} = -\mathrm{Gr}\int_\Omega \left(u_r' w' \frac{\partial u_{r_0}}{\partial z} \right) d\Omega, \tag{20}$$

and

$$I_{v_2} = -\mathrm{Gr}\int_\Omega \left(w' u_r' \frac{\partial w_0}{\partial r} \right) d\Omega. \tag{21}$$

Therefore, the first term Iv_1, which is destabilizing for both values of Pr, measures the amplification of radial velocity disturbances (u_r') by axial transport (w') of axial gradients of the basic radial flow ($\partial u_{r_0}/\partial z$). Similarly, the second term I_{v_2}, which is stabilizing, describes the amplification of axial velocity disturbances (w') by radial transport (u_r') of axial shear ($\partial w_0/\partial r$). The third term I_{v_3}, which is stabilizing, gives the amplification of axial velocity disturbances by axial transport of axial gradients of the basic axial flow.

For Pr=0.02, it is important to notice that all the destabilizing terms, I_b, I_{v_1}, and I_{v_3}, are increasing at the transition, so that they share responsibility for this bifurcation, the main increase being given by I_{v_1} and then connected to axial gradients of the basic radial flow.

The analysis of the thermal energy contributions, given in Fig. 9, confirms the fact that for the low values of Pr, the thermal energy is just a balance between I_{T_3} which measures the amplification of temperature disturbances (T') due to the axial transport (w') of the axial gradient of the basic temperature profile ($\partial T_0/\partial z$), and the heat conduction I_{d_T}. The

variation of I_Θ can also be neglected compared to that of I_k. Then we can conclude that for Pr=0.02, the basic flow becomes unstable because of inertial instability. On the other hand, if we compare the variations of I_Θ and I_k for Pr=1, we can notice that I_Θ increases slightly more quickly than I_k, indicating a preponderance of the thermal mechanisms, even if the inertial effects cannot be neglected.

5. Study of the secondary bifurcation for Pr=6.7

Hardin and Sani[11] found, for Pr=6.7 and $A=0.5$, a transition from the axisymmetric solution to a new solution connected to a $m=2$ perturbation at $\mathrm{Ra}c_2=45\,800$. Figure 10(a) shows that the evolution of the most unstable eigenvalue, corresponding to the mode $m=2$, has a negative maximum at Ra=51 456, confirming the absence of transition to a $m=02$ mode, as already indicated by Wanschura *et al.*[13] The axisymmetric solution is then found to be unstable to a $m=1$ mode at $\mathrm{Ra}c_2=197\,930$ [Fig. 10(b)]. This result agrees qualitatively with Wanschura *et al.*,[13] but this value of $\mathrm{Ra}c_2$ is 22% greater than their value ($\mathrm{Ra}c_2=162\,144$), but less than the value given by the experiment of Müller *et al.*[9] ($\mathrm{Ra}c_2=361\,600$).

The plots giving the energetic contributions around this transition [Figs. 10(c) and 10(d)] show that the dissipation is almost totally counterbalanced by I_b, and that, although I_{T_3} remains the principal source of destabilization, I_{T_1} and I_{T_2} are no more negligible in the thermal energy balance. Comparing the evolution of I_k and I_Θ, we conclude that the instability is due exclusively to thermal mechanisms.

6. Heat transfer

Beyond the onset of convection, the heat transfer can be represented by the Nusselt number defined as

$$\mathrm{Nu}=\frac{4}{\pi}\int_0^{2\pi}\int_0^{1/2}\left(-\frac{\partial T}{\partial z}\right)_{z=A} r\,dr\,d\phi. \tag{22}$$

The secondary bifurcation to the $m=02$ solution is presented in Fig. 11 by a plot of the Nusselt number Nu versus the Rayleigh number Ra, for $A=0.5$ and two values of Pr, Pr=0.02 and Pr=1. For both cases, the heat transfer is greater for the new stable $m=02$ solution. The plot of the temperature field in an axial symmetry plane and the contours of the vertical velocity in the horizontal midplane (Fig. 12), before and beyond the secondary bifurcation, show that qualitatively similar flow patterns are obtained for Pr=0.02 and Pr=1. However, the isotherms are found to be flatter for Pr=0.02 compared to Pr=1. This difference can be attributed to the high thermal conductivity of small-Prandtl-number fluids.

V. CONCLUSIONS

We have presented a three-dimensional numerical study of steady convective flows in a vertical cylindrical cavity heated from below (Rayleigh–Bénard convection). Three types of convective patterns have been observed at the onset of convection: the azimuthal modes $m=0$, $m=1$, and $m=2$. Linear analysis has shown that the pattern corresponding to the emerging flow changes when the aspect ratio A is increased. For $A<0.55$ convection sets in as an axisymmetric mode and for $A>0.55$ as a $m=1$ mode. Symmetry considerations have been used to get information on the type of bifurcation and the number of equivalent solutions for a given mode. As always for Rayleigh–Bénard convection, the primary bifurcations are pitchfork bifurcations because the up–down symmetry is broken by the onset of convection. Bifurcation diagrams have then been presented for two aspect ratios: $A=0.5$ and $A=1$. For $A=0.5$, the emerging flow corresponds to an axisymmetric solution (lowest critical Rayleigh number). It undergoes a secondary bifurcation at which it is destabilized by an $m=2$ eigenmode. The new nonlinear stable steady state, denoted $m=02$, is a convective flow with two parallel rolls. The critical Rayleigh number for the secondary bifurcation is found to increase quadratically at low Prandtl numbers and linearly at larger Prandtl numbers. The energetic analysis of this instability has shown that the bifurcation is due to inertial mechanisms for Pr=0.02, and primarily to thermal mechanisms for Pr=1. For Pr=6.7, the axisymmetric solution is stable to the $m=2$ perturbation, confirming the analysis of Wanschura *et al.*[13] and the numerical simulation of Wagner *et al.*[12] But the basic flow loses stability to an $m=1$ eigenmode at $\mathrm{Ra}c_2=197\,930$, in qualitative agreement with Wanschura *et al.*[13] who found the transition at $\mathrm{Ra}c_2=162\,144$, and with the experimental result of Müller *et al.*[9] ($\mathrm{Ra}c_2=361\,600$). Thermal mechanisms are found to be responsible for this transition at Pr=6.7.

ACKNOWLEDGMENTS

We wish to thank Dr. L. Tuckerman from LIMSI and Dr. A. Bergeon from IMFT for helpful discussions of our results. This work was supported by the ''Centre National des Etudes Spatiales.'' Computations were carried out on a Cray YMP C98 computer, with the support from the CNRS through the IDRIS institute.

[1] L. Rayleigh, Scientific papers, Cambridge Univ. Press **6**, 432 (1916).
[2] H. Bénard, ''Les tourbillons cellulaires dans une nappe de liquide transportant de la chaleur par convection en régime permanent,'' Ann. Chim. Phys. **23**, 62 (1901).
[3] G. S. Charlson and R. L. Sani, ''Thermoconvective instability in a bounded cylindrical fluid layer,'' Int. J. Heat Mass Transf. **13**, 1479 (1970).
[4] G. S. Charlson and R. L. Sani, ''On thermoconvective instability in a bounded cylindrical fluid layer,'' Int. J. Heat Mass Transf. **14**, 2157 (1971).
[5] K. Stork and U. Müller, ''Convection in boxes: An experimental investigation in vertical cylinders and annuli,'' J. Fluid Mech. **71**, 231 (1975).
[6] S. Rosenblat, ''Thermal convection in a vertical circular cylinder,'' J. Fluid Mech. **122**, 395 (1982).
[7] J. C. Buell and I. Catton, ''The effect of wall conduction on the stability of a fluid in a right circular cylinder heated from below,'' J. Heat Transfer **105**, 255 (1983).
[8] G. S. Charlson and R. L. Sani, ''Finite amplitude axisymmetric thermoconvective flows in a bounded cylindrical layer of fluid,'' J. Fluid Mech. **71**, 209 (1975).
[9] G. Müller, G. Neumann, and W. Weber, ''Natural convection in vertical Bridgman configurations,'' J. Cryst. Growth **70**, 78 (1984).
[10] G. Neumann, ''Three-dimensional numerical simulation of buoyancy-driven convection in vertical cylinders heated from below,'' J. Fluid Mech. **214**, 559 (1990).

[11]G. R. Hardin and R. L. Sani, ''Buoyancy-driven instability in a vertical cylinder: Binary fluids with Soret effect. Part 2: Weakly non-linear solutions,'' Int. J. Numer. Methods Fluids **17**, 755 (1993).
[12]C. Wagner, R. Friedrich, and R. Narayanan, ''Comments on the numerical investigation of Rayleigh and Marangoni convection in a vertical cylinder,'' Phys. Fluids **6**, 1425 (1994).
[13]M. Wanschura, H. C. Kuhlmann, and H. J. Rath, ''Three-dimensional instability of axisymmetric buoyant convection in cylinders heated from below,'' J. Fluid Mech. **326**, 399 (1996).
[14]M. Golubitsky, I. Stewart, and D. Schaeffer, *Singularities and groups in bifurcation theory, Vol. II* (Springer Verlag, New York, 1988).
[15]J. D. Crawford and E. Knobloch, ''Symmetry and symmetry-breaking in fluid dynamics,'' Annu. Rev. Fluid Mech. **23**, 341 (1991).
[16]A. Bergeon, D. Henry, H. BenHadid, and L. S. Tuckerman, ''Marangoni convection in binary mixtures with Soret effect,'' J. Fluid Mech. **375**, 143 (1998).
[17]G. E. Karniadakis, M. Israeli, and S. A. Orszag, ''High-order splitting method for the incompressible Navier-Stokes equations,'' J. Comput. Phys. **97**, 414 (1991).
[18]T. C. Oppe, W. D. Joubert, and D. R. Kincaid, ''NSPCG, a package for solving large sparse linear systems by various iterative methods,'' Center for Numerical Analysis, University of Texas at Austin (1989).
[19]C. K. Mamun and L. S. Tuckerman, ''Asymmetry and Hopf bifurcation in spherical Couette flow,'' Phys. Fluids **7**, 80 (1995).
[20]H. B. Keller, ''Numerical solution of bifurcation and nonlinear eigenvalue problems,'' *Applications of Bifurcation Theory*, edited by P. Rabinowitz (Academic, New York, 1977).
[21]R. Touihri, ''Stabilité des écoulements dans une cavité cylindrique chauffée par le bas en présence d'un champ magnétique,'' Ph.D. Thesis, Ecole Centrale de Lyon, 1998.
[22]N. Nayar and J. M. Ortega, ''Computation of selected eigenvalues of generalized eigenvalue problems,'' J. Comput. Phys. **108**, 8 (1993).
[23]A. T. Patera, ''A spectral element method for fluid dynamics: Laminar flow in a channel expansion,'' J. Comput. Phys. **54**, 468 (1984).
[24]K. Z. Korczak and A. T. Patera, ''An isoparametric spectral element method for solution of the Navier-Stokes equations in complex geometry,'' J. Comput. Phys. **62**, 361 (1986).
[25]G. Z. Gershuni and E. M. Zhukhovitskii, *Convective stability of incompressible fluids* (Keterpress Entreprise, Jerusalem, 1976).